

SPECTRAL DOMAIN ANALYSIS OF A CIRCULAR NANO-APERTURE ILLUMINATING A PLANAR LAYERED SAMPLE

K. A. Michalski

Department of Electrical and Computer Engineering
Texas A&M University, College Station, TX 77843-3128, USA

Abstract—A rigorous and efficient spectral domain formalism is presented of a plane wave-excited subwavelength circular aperture in a planar perfectly conducting metallic screen of infinitesimal thickness, based on the Bethe-Bouwkamp quasi-static model. The formulation utilizes a transmission line analogue of the medium, which facilitates the inclusion of planar multilayered material samples, where the latter may exhibit uniaxial anisotropy. The transmitted field components are expressed in terms of one-dimensional Hankel transform integrals, which can be evaluated by efficient numerical procedures. Sample results are presented showing the intensity profiles and polarization states of transmitted light penetrating into a semiconductor layer.

1. INTRODUCTION

The problem of light transmission through a subwavelength circular aperture in a metallic screen has been of much interest in the context of scanning near-field optical microscopy (SNOM). The first solution—assuming a perfectly conducting screen of infinitesimal thickness and an aperture of radius $a \ll \lambda$, where λ is the wavelength—was put forward by Bethe [1], and later corrected by Bouwkamp [2, 3], who derived a quasi-static expression for the equivalent magnetic current of the aperture. With the latter known, the transmitted field can be solved for in either the space domain or the Fourier spectrum domain. The first numerical studies of the transmitted light based on the Bethe-Bouwkamp (BB) quasi-static model employed the space domain approach [4–6]. The disadvantage of this method is that it cannot

readily be extended to include the effect of a nearby material sample and it becomes cumbersome for anisotropic media. These limitations are easily overcome if the solution is pursued in the Fourier spectrum domain, since individual modes can be propagated through dielectric interfaces using the Fresnel equations. Also, the uniaxial anisotropy is only a minor complication in the spectral domain, since the transverse-magnetic (TM) and transverse-electric (TE) partial fields can be decoupled and propagated separately. The sources of these partial fields are determined by the spectrum of the BB equivalent magnetic current of the aperture. Consequently, the spectral domain approach based on the BB model has frequently been used in the SNOM context [7–17], and some of these works included the effect of a nearby planar material sample in the formulation. Baida and Van Labeke [15] also converted the Cartesian Fourier transform representation into a more efficient Fourier-Bessel transform representation, which replaces the two-dimensional Fourier-type integrals by one-dimensional Hankel transforms. The advantage of the latter representation was earlier recognized by Grober et al. [10], who derived the spectral sources of the TE and TM partial fields from the Fourier transforms of the BB expressions for, respectively, the normal magnetic and electric field components in the aperture plane. However, their TM source expressions are approximate. Recently, Michalski [18] used the BB model in conjunction with the complex image method to analyze subwavelength circular apertures under oblique incidence.

In the present paper, we extend the works of Grober et al. [10] and Van Labeke et al. [12,15] and present an efficient spectral domain method for the analysis of a subwavelength circular aperture nanosource illuminating a planar material sample, where the latter may be layered and uniaxially anisotropic, with the optic axis perpendicular to the stratification. Our formulation is exact and it utilizes a transmission line analogue of the medium, which facilitates an efficient treatment of multilayered samples. The proposed method is applicable to experiments in SNOM when flat samples are evaluated, as well as in studies of metamaterial and metallodielectric multilayers for superlensing and superguidance applications at optical frequencies [19, 20].

2. STATEMENT OF THE PROBLEM

The structure under consideration is illustrated in Fig. 1, where we assume that the screen and the material sample are of infinite lateral extent. The screen is perfectly conducting and of infinitesimal thickness, and the aperture is circular with a subwavelength radius.

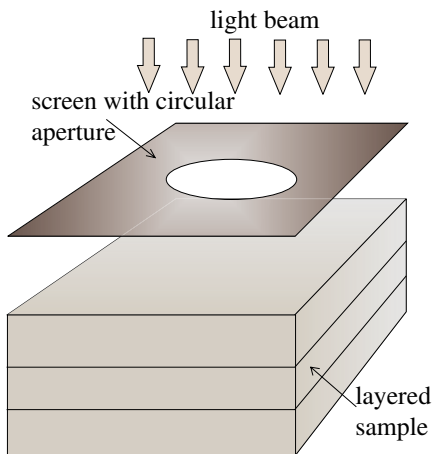


Figure 1. Schematic diagram of a plane wave-excited circular aperture in a presence of a layered sample.

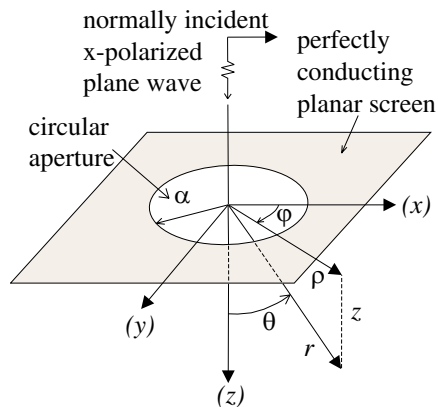


Figure 2. Diagram of a plane wave impinging on a circular aperture in a planar screen, indicating the coordinate system used in the analysis.

The sample may comprise any number of layers and may be uniaxially anisotropic, with the optic axis perpendicular to the stratification, and is characterized by piecewise-constant transverse and axial permittivities ϵ and ϵ_z , and transverse and axial permeabilities μ and μ_z . The incident field geometry and the coordinate system employed are illustrated in Fig. 2. The aperture is excited by a unit-strength, x -polarized plane wave propagating along the z axis.

In view of the field equivalence principle, the knowledge of the tangential electric field E_t in the plane of the screen ($z = 0$) is sufficient to determine the electromagnetic field at any point in the $z > 0$ half-space [21, p. 110]. In the equivalent problem the aperture is shorted and a magnetic surface current with density $M_S = E_t \times z$ is placed over the area $\rho < a$ previously occupied by the aperture. (Note that we distinguish unit vectors by carets.) According to the BB quasi-static theory, applicable for $a \ll \lambda$, this M_S is given as [3]

$$M_S = -\frac{8jka}{3\pi} \left(\hat{\rho} \sqrt{1 - \xi^2} \sin \varphi + \hat{\varphi} \frac{2 - \xi^2}{2\sqrt{1 - \xi^2}} \cos \varphi \right), \quad (1)$$

where $k = 2\pi/\lambda$ is the wavenumber and $\xi = \rho/a < 1$ is the normalized radial coordinate. We assume the e^{jwt} time convention and SI units.

3. SPECTRAL DOMAIN FORMULATION

In order to compute the electromagnetic field due to the equivalent magnetic current M_S backed by the screen and facing the layered sample, we perform a transverse-longitudinal decomposition of the Maxwell's equations [22, p. 386] and eliminate the transverse field components in favor of the longitudinal ones. Then, we apply a Fourier transformation in the transverse plane, which in effect reduces the problem to a one-dimensional one along the z axis. Since the structure is of infinite lateral extent and it includes the origin, where the fields should not diverge, any field component may be expressed as (cf. [23, p. 48])

$$f(\rho, \varphi) = \sum_{n=0}^{\infty} \left[\cos n\varphi {}_n\mathcal{F}_n^c\{\tilde{f}_n^c(k_\rho)\} + \sin n\varphi \mathcal{S}_n\{\tilde{f}_n^s(k_\rho)\} \right], \quad (2)$$

with

$$\tilde{f}_n^s(k_\rho) \equiv \mathcal{F}_n^s\{f(\rho, \varphi)\} = \mathcal{S}_n^{-1} \left\{ \frac{\varepsilon_n}{2\pi} \int_{-\pi}^{\pi} d\varphi \frac{\cos n\varphi}{\sin n\varphi} f(\rho, \varphi) \right\}, \quad (3)$$

where ε_n is the Neumann number ($\varepsilon_n = 1$ for $n = 0$ and $\varepsilon_n = 2$ for $n > 0$). In the above, we utilize the Fourier-Bessel transform pair (cf. [24, p. 21])

$$\mathcal{S}_n\{\cdot\} \equiv \int_0^{\infty} dk_\rho k_\rho J_n(k_\rho \rho) \{\cdot\}, \quad (4)$$

$$\mathcal{S}_n^{-1}\{\cdot\} \equiv \int_0^{\infty} d\rho \rho J_n(k_\rho \rho) \{\cdot\}, \quad (5)$$

where k_ρ is the spectral domain counterpart of ρ and J_n is the Bessel function of order n . The transforms (4) and (5) will also be referred to as the Hankel transform of order n and its inverse, respectively.

It then follows from the Maxwell's equations that the BB magnetic current (1) only excites the $n = 1$ even-TM and $n = 1$ odd-TE modes. Consequently, the normal field components may be expressed as

$$E_z = \frac{\cos \varphi}{jw\epsilon_z} \mathcal{S}_1\{I^e(k_\rho, z)\}, \quad (6)$$

$$H_z = -\frac{\sin \varphi}{jw\mu_z} \mathcal{S}_1\{V^h(k_\rho, z)\}, \quad (7)$$

from which the transverse fields follow as

$$E_\rho = -\cos \varphi \int_0^{\infty} dk_\rho \left[J_1'(k_\rho \rho) V^e(k_\rho, z) - \frac{J_1(k_\rho \rho)}{k_\rho \rho} V^h(k_\rho, z) \right], \quad (8)$$

$$E_\varphi = \sin \varphi \int_0^\infty dk_\rho \left[\frac{J_1(k_\rho \rho)}{k_\rho \rho} V^e(k_\rho, z) - J'_1(k_\rho \rho) V^h(k_\rho, z) \right], \quad (9)$$

$$H_\rho = -\sin \varphi \int_0^\infty dk_\rho \left[\frac{J_1(k_\rho \rho)}{k_\rho \rho} I^e(k_\rho, z) - J'_1(k_\rho \rho) I^h(k_\rho, z) \right], \quad (10)$$

$$H_\varphi = -\cos \varphi \int_0^\infty dk_\rho \left[J'_1(k_\rho \rho) I^e(k_\rho, z) - \frac{J_1(k_\rho \rho)}{k_\rho \rho} I^h(k_\rho, z) \right], \quad (11)$$

where primes indicate derivatives with respect to the argument. The functions V^α and I^α introduced above, with $\alpha = e, h$, satisfy the transmission line equations

$$\frac{dV^\alpha}{dz} = -jk_z^\alpha Z^\alpha I^\alpha + v^\alpha, \quad (12a)$$

$$\frac{dI^\alpha}{dz} = -jk_z^\alpha Y^\alpha V^\alpha, \quad (12b)$$

where

$$k_z^\alpha = \sqrt{k^2 - k_\rho^2 / \nu^\alpha}, \quad \Im k_z^\alpha \leq 0, \quad (13)$$

$$Z^e = \eta \frac{k_z^e}{k}, \quad Z^h = \eta \frac{k}{k_z^h}, \quad (14)$$

with $Y^\alpha = 1/Z^\alpha$. In the above, $k = \omega \sqrt{\mu \epsilon}$ and $\eta = \sqrt{\mu / \epsilon}$ are the (transverse) wavenumber and intrinsic impedance, respectively, and

$$\nu^e = \frac{\epsilon_z}{\epsilon}, \quad \nu^h = \frac{\mu_z}{\mu}, \quad (15)$$

are the electric and magnetic anisotropy ratios of the medium. It is understood that these parameters are evaluated at z . Note that, as already anticipated by the notation, V^α and I^α may be interpreted as the voltage and current on a transmission line with the propagation constant k_z^α and characteristic impedance Z^α , excited by a voltage source v^α . The transmission lines corresponding to $\alpha = e$ and $\alpha = h$ characterize the TM and TE partial fields, respectively. Their propagation constants k_z^α are different, unless the medium is isotropic ($\nu^\alpha = 1$). Since the magnetic current (1) resides at $z = 0$, the corresponding transmission line voltage sources are impulsive and may be expressed as

$$v^\alpha(k_\rho, z) = V_g^\alpha(k_\rho) \delta(z), \quad (16)$$

where δ is the Dirac delta and $V_g^\alpha(k_\rho)$ are the voltages of lumped generators located at $z = 0$ on the TM ($\alpha = e$) or TE ($\alpha = h$) transmission line. The voltages of the TM and TE transmission line

generators can be found as

$$V_g^e(k_\rho) = \mathcal{F}_1^c \{ -\nabla_t \cdot (M_S \times \hat{z}) \} = -\frac{4jka^3}{3\pi} F_0(k_\rho a) k_\rho, \quad (17)$$

$$V_g^h(k_\rho) = \mathcal{F}_1^s \{ \nabla_t \cdot M_S \} = \frac{4jka^3}{3\pi} F_1(k_\rho a) k_\rho, \quad (18)$$

where \mathcal{F}_1^c and \mathcal{F}_1^s are the first-order cosine and sine transforms defined in (3). In the above, we have used the BB magnetic surface current (1) and the notation

$$F_0(k_\rho a) = j_0(k_\rho a), \quad F_1(k_\rho a) = 3 \frac{j_1(k_\rho a)}{k_\rho a}. \quad (19)$$

For later convenience, we also define the difference function

$$F_2(k_\rho a) = F_1(k_\rho a) - F_0(k_\rho a) = j_2(k_\rho a), \quad (20)$$

which appears in the field expressions for isotropic homogeneous media. In these formulas, j_n denotes the spherical Bessel functions of order n . The functions F_i , $i = 0, 1, 2$, which we refer to as the aperture source functions, are plotted in Fig. 3. In interpreting these plots, one should bear in mind that F_0 and F_1 excite the TM and TE partial fields, and that the small and large spatial frequencies correspond to the far- and near-zone regions in the space domain, respectively.

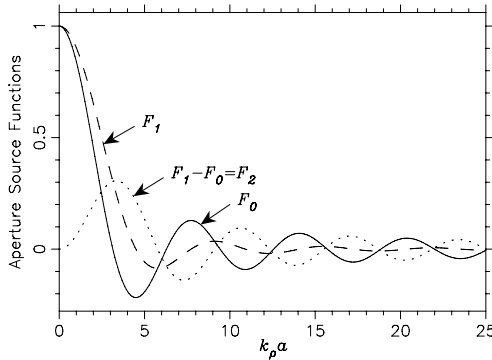


Figure 3. Plot of the aperture source functions.

It should be noted that Grober et al. [10] previously derived expressions equivalent to our (17), (18) using a less direct approach, involving approximations in the TM case. In Appendix A, we briefly discuss the Grober et al. method and compare their approximate TM source with the exact one presented here.

The equivalent transmission line network for the geometry of Fig. 1 is illustrated in Fig. 4, where the short circuit represents the

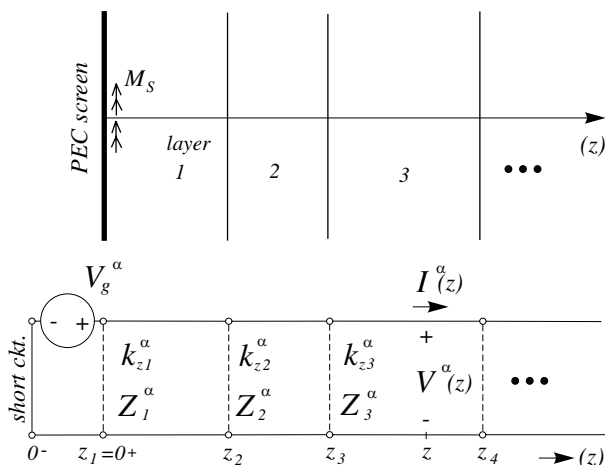


Figure 4. Schematic diagram of the aperture-excited layered sample and its transmission line analogue. For simplicity, the dependence on k_ρ is not explicitly indicated.

perfectly conducting screen and the layered medium is replaced by a tandem connection of transmission line sections. Since the material sample begins with layer 2, layer 1 is in our problem isotropic and the propagation constant of the corresponding transmission line section is

$$k_z = \sqrt{k^2 - k_\rho^2}, \quad \Im m k_z \leq 0. \tag{21}$$

The transmission line voltages and currents excited by the voltage generators V_g^α readily follow once the TM and TE transmission line Green functions are determined, where the latter are simply the voltage and current corresponding to $V_g^\alpha = 1$ in Fig. 4. Hence, if we denote these Green functions by $V_v^\alpha(k_\rho; z|z')$ and $I_v^\alpha(k_\rho; z|z')$, we may write

$$V^\alpha(k_\rho, z) = V_g^\alpha(k_\rho) V_v^\alpha(k_\rho; z|0), \tag{22}$$

$$I^\alpha(k_\rho, z) = V_g^\alpha(k_\rho) I_v^\alpha(k_\rho; z|0), \tag{23}$$

since in our case the voltage source is always at $z' = 0$. The transmission line Green functions for uniaxial multilayers can readily be found, as discussed in Appendix B.

Upon using (22), (23) in conjunction with (17), (18) in (6)–(11), more explicit expressions for the fields can be derived. Namely, upon using the recurrence relations for the Bessel functions, the Cartesian

field components may be expressed as

$$E_x = \frac{2jka^3}{3\pi} \left[\mathcal{S}_0\{F_1 V_v^h + F_0 V_v^e\} + \cos 2\varphi \mathcal{S}_2\{F_1 V_v^h - F_0 V_v^e\} \right], \quad (24)$$

$$E_y = \frac{2jka^3}{3\pi} \sin 2\varphi \mathcal{S}_2\{F_1 V_v^h - F_0 V_v^e\}, \quad (25)$$

$$E_z = -\frac{4ka^3}{3\pi} \cos \varphi \mathcal{S}_1\{F_0 k_\rho \mathcal{I}_v^e\}, \quad (26)$$

$$H_x = -\frac{2jka^3}{3\pi} \sin 2\varphi \mathcal{S}_2\{F_1 I_v^h - F_0 I_v^e\}, \quad (27)$$

$$H_y = \frac{2jka^3}{3\pi} \left[\mathcal{S}_0\{F_1 I_v^h + F_0 I_v^e\} + \cos 2\varphi \mathcal{S}_2\{F_1 I_v^h - F_0 I_v^e\} \right], \quad (28)$$

$$H_z = -\frac{4ka^3}{3\pi} \sin \varphi \mathcal{S}_1\{F_1 k_\rho \mathcal{V}_v^h\}, \quad (29)$$

where we have omitted the function arguments for notational simplicity. In (26) and (29) we have introduced the normalized quantities

$$\mathcal{I}_v^e \equiv \frac{\eta}{k\nu^e} I_v^e, \quad \mathcal{V}_v^h \equiv \frac{1}{\eta k\nu^h} V_v^h, \quad (30)$$

where it is understood that η , k , and ν^α are evaluated at z . The Hankel transform integrals in (24)–(29) can be computed by an efficient scheme based on adaptive quadrature with extrapolation [25].

If the medium is isotropic and homogeneous, which is the case considered by Grober et al. [10], there are no reflections, and the transmission line Green functions may be written by inspection of the equivalent circuit of Fig. 4 as

$$V_v^\alpha(k_\rho; z|0) = e^{-jk_z z}, \quad I_v^\alpha(k_\rho; z|0) = Y^\alpha e^{-jk_z z}. \quad (31)$$

In this case, the expressions (24)–(29) can be much simplified, in view of $V_v^e = V_v^h$ and (20).

4. SAMPLE NUMERICAL RESULTS

In Figs. 5–7 we present plots of the time-average Poynting vector

$$\langle \mathbf{S} \rangle = \frac{1}{2} \Re e (\mathbf{E} \times \mathbf{H}^*), \quad (32)$$

in the xz - and yz -planes for an aperture of radius $a = 50$ nm at $\lambda = 600$ nm ($a/\lambda = 0.083$). The vector plots are normalized, in order to clearly show the direction of the power flux not only in the vicinity of the aperture, but also farther from it, where the field strength

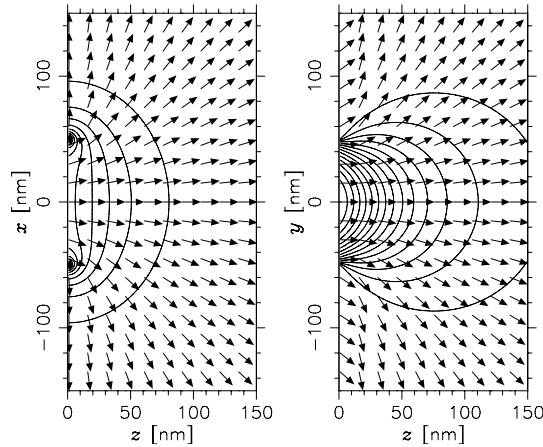


Figure 5. Plots of the time-average Poynting vector $\langle \mathbf{S} \rangle$ in the xz - and yz -planes for $a = 50$ nm at $\lambda = 600$ nm in free space.

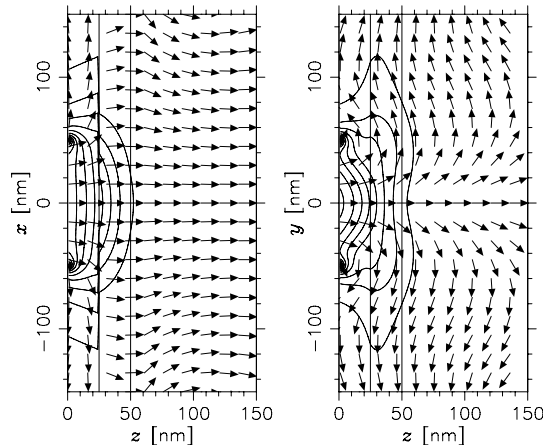


Figure 6. As in Fig. 5, but with a GaAs slab occupying the range $0.5 < z/a < 1$.

decreases precipitously. The magnitude information is conveyed by the constant level contours superposed on the vector plots. The plot in Fig. 5 is for the case of free space, and the plots in Figs. 6, 7 show the effect of a GaAs slab ($\epsilon = 15.326 - j1.568$ [26]) occupying the range $25 < z < 50$ nm ($0.5 < z/a < 1$). In the latter case, we employed the modified transmission line Green functions, which exclude reflections from the infinite screen, as discussed in Appendix B. We have

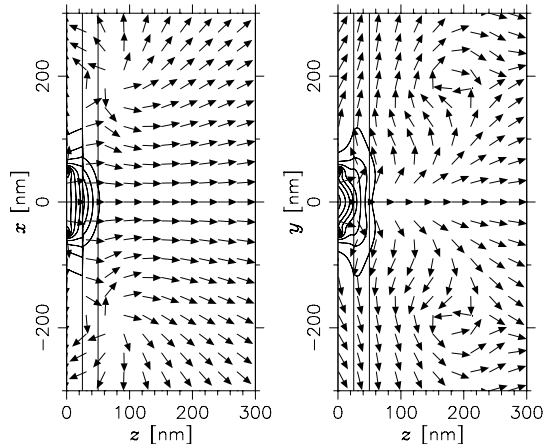


Figure 7. As in Fig. 6, but with an expanded range.

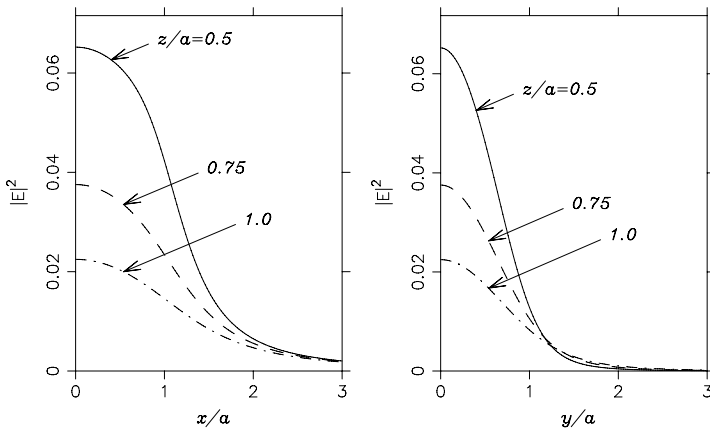


Figure 8. Plots of the electric field intensity $|\mathbf{E}|^2$ along the x - and y -axes for $a = 50$ nm at $\lambda = 600$ nm in free space.

confirmed that our free space results are in excellent agreement with the corresponding results of the space domain method [4], which we have also implemented. The xz -plane results exhibit the expected field singularity near the aperture edges, since the electric field is polarized in the plane of the plot. It is interesting to note that with the slab present, a circulating power flux is observed in Fig. 6. The optical vortices are clearly visible in Fig. 7, where the power flux is plotted in an expanded range. Although these vortices are observed in regions of very small field intensity, they do not appear to be spurious artifacts.

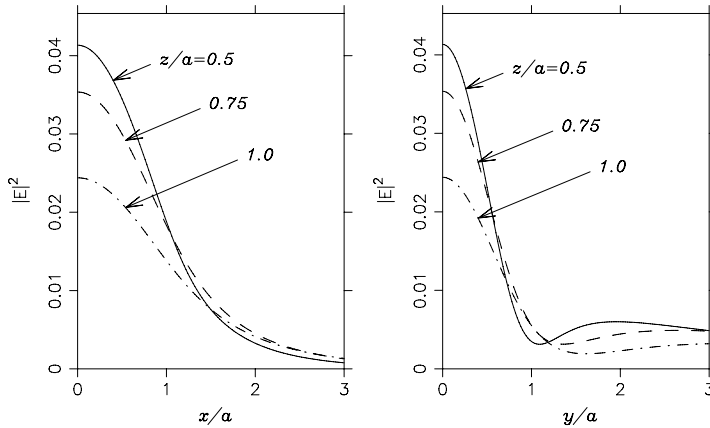


Figure 9. As in Fig. 8, except that the plots are within a GaAs slab occupying the range $0.5 < z/a < 1$.

Such singular points are not uncommon and have been previously observed in a vicinity of a subwavelength slit [27, 28].

For the same aperture size and wavelength, in Figs. 8, 9 we present the squared electric field intensity $|E|^2$ profiles along the x - and y -axes at three distances from the screen: $z/a = 0.5, 0.75$, and 1 . The former is for the free space case, and the latter shows the effect of a GaAs layer, with the three intensity plots computed inside the sample — the first in the front face, the second in the middle plane, and the third in the back face. Similar results were published by Stevenson and Richards [14] for an infinitely thick GaAs sample. Of interest in the SNOM context are the full-width half-maximum (FWHM) values, which define the attainable resolution. As previously noted by Stevenson and Richards, the FWHM is reduced within the semiconductor. Our results indicate that, as compared to the free space case, the field intensity within a finite-thickness slab decreases less rapidly with distance, which can be attributed to the partial field reflection from the back face of the sample. For the infinitely thick GaAs layer, Stevenson and Richards observed the occurrence of two subsidiary maxima in addition to the prominent peak at the center of the intensity plot along the y -axis. These maxima, which could produce two ‘ghost’ images for the scan direction perpendicular to the incident field polarization, are also present in the finite-thickness sample, as the plots of Fig. 9 indicate.

Table 1. Normal field components in the aperture plane.

| | $\xi < 1$ | $\xi > 1$ |
|-------|--|---|
| E_z | 0 | $-\frac{4jka}{3\pi} \frac{1}{\xi\sqrt{\xi^2-1}} \cos \varphi$ |
| H_z | $-\frac{4}{\pi\eta} \frac{\xi}{\sqrt{1-\xi^2}} \sin \varphi$ | 0 |

5. CONCLUSION

A rigorous and efficient spectral domain formulation is presented for the analysis of a subwavelength circular aperture nanosource illuminating a planar material sample, where the latter may be layered and uniaxially anisotropic. Our formulation is based on the Bethe-Bouwkamp quasi-static aperture model and utilizes a transmission line analogue of the medium, which facilitates the inclusion of multilayered structures. Sample results are presented showing the intensity profiles and polarization states of transmitted light penetrating into a semiconductor layer. The proposed method is well-suited for the modeling of the observations in scanning near-field optical microscopy (SNOM) when relatively flat samples are evaluated, as well as in the studies of metamaterial and metallodielectric multilayers for superlensing and superguiding applications at optical frequencies.

APPENDIX A. THE METHOD OF GROBER ET AL. [10]

Our approach is based on the field equivalence theorem, which allows the fields in a region of space to be uniquely determined from the *tangential* field components \mathbf{E}_t on the boundary surface of the region. However, according to one variant of the vector Huygens principle, the knowledge of the *normal* field components ($\mathbf{E}_n, \mathbf{H}_n$) on a closed surface is also sufficient to determine the fields within [29]. This was the basis of the Grober et al. [10] formulation, who used the knowledge of (E_z, H_z) in the $z = 0$ plane to derive the electromagnetic field in the $z > 0$ half-space. Grober et al. employed the Bouwkamp [2] quasi static field expressions given in Table 1 as the point of departure. Pursuing this approach, we note upon inspection of Fig. 4 that the spectral source of the TE partial field is $V_g^h(k_\rho) \equiv V^h(k_\rho, 0^+)$. Hence, in view of (7), $V_g^h(k_\rho)$ may be obtained from H_z by the Fourier-Bessel transform (3) in the $z = 0$ plane. Using the H_z expression of Table 1, we find that the resulting $V_g^h(k_\rho)$ is given by (18) obtained earlier. Turning attention to the source of the TM partial field, we note that in view of (6), $I^e(k_\rho, 0^+)$ may be obtained as the Fourier-Bessel transform

of E_z in the $z = 0$ plane. However, the E_z expression of Table 1 is only correct in the vicinity of the aperture, and thus leads to a solution, which is subject to the same restriction. To remedy this, Grober et al. proposed to modify the E_z expression of Table 1 as

$$E_z = -\frac{4jka}{3\pi} e^{-jka\xi} \left(\frac{1}{\xi\sqrt{\xi^2 - 1}} + \frac{jka}{\xi} \right) \cos \varphi. \quad (\text{A1})$$

(They also included a factor e^{jka} , which we omit here, as we have not found this to have any noticeable beneficial effect.) Upon applying the Fourier-Bessel transform (3) to (A1), we find

$$I^e(k_\rho, 0^+) = \frac{4k^2 a^3}{3\pi\eta} \int_1^\infty d\xi J_1(k_\rho a \xi) e^{-jka\xi} \left(\frac{1}{\sqrt{\xi^2 - 1}} + jka \right), \quad (\text{A2})$$

which is not amenable to exact analytical integration. To overcome this impasse, Grober et al. resorted to some judicious ad hoc approximations in the $k_\rho < k$ (far zone) and $k_\rho > k$ (near zone) ranges, which lead to

$$I^e(k_\rho, 0^+) \approx \frac{4k^2 a^3}{3\pi\eta} \begin{cases} \frac{k_\rho}{jk_z} & \text{if } k_\rho < k, \\ \frac{k_\rho}{jk_z} - 1 + j_0(k_\rho a) & \text{if } k_\rho > k, \end{cases} \quad (\text{A3})$$

where k_z is given in (21). This result should be compared with the exact expression

$$I^e(k_\rho, 0^+) = Y^e V_g^e(k_\rho) = \frac{4k^2 a^3}{3\pi\eta} \frac{k_\rho}{jk_z} j_0(k_\rho a), \quad (\text{A4})$$

which follows from (23), (31) and (17). It is clear that the two formulas asymptotically agree in the small- and large- k_ρ ranges. This is confirmed by the results presented in Fig. A1, where (A3) and (A4) are plotted for an aperture with a diameter of $\lambda/10$, also investigated by Grober et al. [10]. As could be expected, some discrepancy is observed in the intermediate spectral range. However, the impact of this relatively small error in the spectral domain on the accuracy of the resulting space domain field expressions is difficult to quantize a priori.

APPENDIX B. TRANSMISSION LINE GREEN FUNCTIONS

The transmission line (TL) Green functions $V_v^\alpha(k_\rho; z|z')$ and $I_v^\alpha(k_\rho; z|z')$ are the voltage and current, respectively, at z due to a unit-strength voltage source at z' . Since in our case $z' = 0$, we can

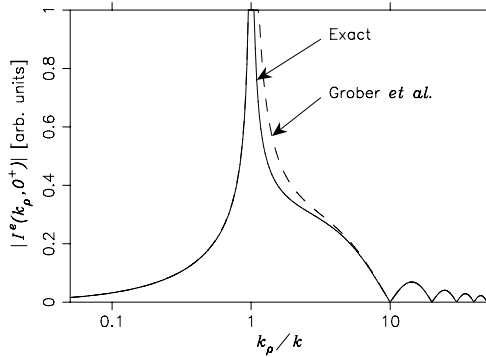


Figure A1. Magnitude of $I^e(k_\rho, 0^+)$ for $2a = \lambda/10$.

find these Green functions by letting $V_g^\alpha = 1$ in the transmission line analogue of Fig. 4. For notational simplicity, henceforth we omit the superscripts α and do not explicitly indicate the dependence of the TL Green functions on k_ρ and z' . If the observation point z is on the n th TL section, the corresponding voltage and current will be denoted by $V_n(z)$ and $I_n(z)$, respectively, and the voltage at the junction point z_n will be denoted by V_n . It can readily be shown that [30]

$$\left. \begin{array}{l} V_n(z) \\ Z_n I_n(z) \end{array} \right\} = \frac{V_n e^{-jk_{zn}(z-z_n)}}{1 + \Gamma_n e^{-j2\theta_n}} \left[1 \pm \Gamma_n e^{-j2k_{zn}(z_{n+1}-z)} \right], \quad (\text{B1})$$

where $\theta_n = k_{zn}d_n$, k_{zn} is the propagation constant of layer n , defined in (14), and $d_n = z_{n+1} - z_n$ is its thickness. In the above, the upper and lower signs in the right-hand expression correspond to the upper and lower expressions on the left, Z_n is the characteristic impedance of the n th TL section, defined in (14), and Γ_n is the voltage reflection coefficient looking out of the right terminal of section n . If there are N TL sections, the last section is reflectionless, hence we set $\Gamma_N = 0$. The other reflection coefficients may then be computed recursively as

$$\Gamma_{n-1} = \frac{R_{n-1} + \Gamma_n e^{-j2\theta_n}}{1 + R_{n-1}\Gamma_n e^{-j2\theta_n}}, \quad n = N, N-1, \dots, 2, \quad (\text{B2})$$

where R_n is the Fresnel reflection coefficient at the n th interface, given as

$$R_n = \frac{Z_{n+1} - Z_n}{Z_{n+1} + Z_n}. \quad (\text{B3})$$

The terminal voltages V_n in (B1) can be found by the recursion

$$V_{n+1} = V_n T_n, \quad n = 1, \dots, N-1, \quad (\text{B4})$$

where $V_1 = 1$ and T_n is the right-looking voltage transmission coefficient across the n th TL section, given as

$$T_n = \frac{V_{n+1}}{V_n} = \frac{(1 + \Gamma_n) e^{-j\theta_n}}{1 + \Gamma_n e^{-j2\theta_n}}. \quad (\text{B5})$$

If it is desired to omit the effect of the infinite screen in Fig. 1 on the scattered field, which may be the case in some SNOM applications, the short-circuit in the TL analogue of Fig. 4 should be replaced by a matched load impedance Z_1 . This change can be implemented by setting

$$V_1 = 1 + \Gamma_1 e^{-j2\theta_1}. \quad (\text{B6})$$

REFERENCES

1. Bethe, H. A., "Theory of diffraction by small holes," *Phys. Rev.*, Vol. 66, 163–182, Oct. 1944.
2. Bouwkamp, C. J., "On Bethe's theory of diffraction by small holes," *Philips Res. Rep.*, Vol. 5, 321–332, Oct. 1950.
3. Bouwkamp, C. J., "Diffraction theory," *Rep. Progr. Phys.*, Vol. 17, 35–100, 1954.
4. Leviatan, Y., "Study of near-zone fields of a small aperture," *J. Appl. Phys.*, Vol. 60, No. 5, 1577–1583, 1986.
5. Dürig, U., D. W. Pohl, and F. Rohner, "Near-field optical-scanning microscopy," *J. Appl. Phys.*, Vol. 59, No. 10, 3318–3327, 1986.
6. Nakano, T. and S. Kawata, "Numerical analysis of the near-field diffraction pattern of a small aperture," *J. Mod. Opt.*, Vol. 39, No. 3, 645–661, 1992.
7. Betzig, E. and R. J. Chichester, "Single molecules observed by near-field scanning optical microscopy," *Science*, Vol. 262, 1422–1425, 1993.
8. Van Labeke, D., D. Barchiesi, and F. Baida, "Optical characterization of nanosources used in scanning near-field optical microscopy," *J. Opt. Soc. Am. A*, Vol. 12, No. 4, 695–703, 1995.
9. Van Labeke, D., F. Baida, D. Barchiesi, and D. Courjon, "A theoretical model for the Inverse Scanning Tunneling Optical Microscope (ISTOM)," *Opt. Commun.*, Vol. 114, 470–480, 1995.
10. Grober, R. D., T. Rutherford, and T. D. Harris, "Modal approximation for the electromagnetic field of a near-field optical probe," *Appl. Opt.*, Vol. 35, 3488–3494, Jul. 1996.
11. Decca, R. S., H. D. Drew, and K. L. Empson, "Investigation of the electric-field distribution at the subwavelength aperture of a

- near-field scanning optical microscope,” *Appl. Phys. Lett.*, Vol. 70, No. 15, 1932–1934, 1997.
12. Van Labeke, D., F. I. Baida, and J. Vigoureux, “A theoretical study of near-field detection and excitation of surface plasmons,” *Ultramicroscopy*, Vol. 71, 351–359, 1998.
 13. Bryant, G. W., E. L. Shirley, L. S. Goldner, E. B. McDaniel, J. W. P. Hsu, and R. J. Tonucci, “Theory of probing a photonic crystal with transmission near-field optical microscopy,” *Phys. Rev. B*, Vol. 58, No. 4, 2131–2141, 1998.
 14. Stevenson, R. and D. Richards, “The use of a near-field probe for the study of semiconductor heterostructures,” *Semicond. Sci. Technol.*, Vol. 13, 882–886, 1998.
 15. Baida, F. I. and D. Van Labeke, “Propagation and diffraction of locally excited surface plasmons,” *J. Opt. Soc. Am. A*, Vol. 18, 1552–1561, Jul. 2001.
 16. Ducourtieux, S., S. Grésillon, J. C. Rivoal, C. Vannier, C. Bainier, D. Courjon, and H. Cory, “Imaging subwavelength holes in chromium films in scanning near-field optical microscopy. Comparison between experiments and calculation,” *Eur. Phys. J. Appl. Phys.*, Vol. 26, 35–43, 2004.
 17. Lin, Y., M. H. Hong, W. J. Wang, Z. B. Wang, G. X. Chen, Q. Xie, L. S. Tan, and T. C. Chong, “Surface nanostructuring by femtosecond laser irradiation through near-field scanning optical microscopy,” *Sens. Actuators A*, Vol. 133, 311–316, 2007.
 18. Michalski, K. A., “Complex image method analysis of a plane wave-excited subwavelength circular aperture in a planar screen,” *Progress In Electromagnetics Research B*, Vol. 27, 253–272, 2011.
 19. Bloemer, M. J., G. D’Aguanno, M. Scalora, N. Mattiucci, and D. de Ceglia, “Energy considerations for a superlens based on metal/dielectric multilayers,” *Opt. Expr.*, Vol. 16, No. 23, 19342–19353, 2008.
 20. De Ceglia, D., M. A. Vincenti, M. G. Cappeddu, M. Centini, N. Akozbek, A. D’Orazio, J. W. Haus, M. J. Bloemer, and M. Scalora, “Tailoring metallodielectric structures for superresolution and superguiding applications in the visible and near-ir ranges,” *Phys. Rev. A*, Vol. 77, 033848-1–12, 2008.
 21. Harrington, R. F., *Time-Harmonic Electromagnetic Fields*, McGraw-Hill, New York, 1961.
 22. Rothwell, E. J. and M. J. Cloud, *Electromagnetics*, 2nd Edition, CRC Press, Boca Raton, FL, 2009.
 23. Iizuka, K., *Engineering Optics*, 2nd edition, Springer-Verlag, New

- York, 1987.
24. Tyras, G., *Radiation and Propagation of Electromagnetic Waves*, Academic Press, New York, 1969.
 25. Michalski, K. A., "Extrapolation methods for Sommerfeld integral tails (Invited review paper)," *IEEE Trans. Antennas Propagat.*, Vol. 46, 1405–1418, Oct. 1998.
 26. Palik, E. D., Editor, *Handbook of Optical Constants of Solids*, Vol. 1, Academic Press, San Diego, 1998.
 27. Schouten, H. F., T. D. Visser, D. Lenstra, and H. Blok, "Light transmission through a suwavelength slit: Waveguiding and optical vortices," *Phys. Rev. E*, Vol. 67, 036608-1–4, 2003.
 28. D'Aguanno, G., N. Mattiucci, M. Bloemer, and A. Desyatnikov, "Optical vortices during a superresolution process in a metamaterial," *Phys. Rev. A*, Vol. 77, 043825-1–4, 2008.
 29. Rumsey, V. H., "Some new forms of the Huygens' principle," *IEEE Trans. Antennas Propagat.*, Vol. 7, S103–S115, Dec. 1959.
 30. Michalski, K. A., "Electromagnetic field computation in planar multilayers," *Encyclopedia of RF and Microwave Engineering*, K. Chang, Editor, Vol. 2, 1163–1190, Wiley-Interscience, 2005.